Astron. Astrophys. 324, 311–323 (1997)

ASTRONOMY
AND
ASTROPHYSICS

Convection driven heating of the solar middle chromosphere by resistive dissipation of large scale electric currents

Michael L. Goodman

Computer Sciences Corporation Code 695 NASA Goddard Space Flight Center Greenbelt, Maryland 20771, USA
(goodman@spof02.gsfc.nasa.gov)

Received 2 December 1996 / Accepted 6 January 1997

Abstract. A two dimensional, steady state, resistive magnetohydrodynamic (MHD) model with flow is used to support the proposition that a major source of heating for the solar middle chromosphere is resistive dissipation of large scale electric currents driven by a convection electric field. The currents are large scale in that their scale heights range from hundreds of kilometers in the network to thousands of kilometers in the internetwork. The current is carried by protons, and flows orthogonal to the magnetic field in a weakly ionized, strongly magnetized hydrogen plasma. The flow velocity is mainly parallel to the magnetic field. The relatively small component of flow velocity orthogonal to the magnetic field generates a convection electric field which drives the current. The magnetic field is the sum of a loop shaped field, called a magnetic element, and a much stronger, larger scale potential field. All of the heating takes place in the magnetic element. Solutions to the model indicate that magnetic elements with horizontal spatial extents of about one thousand to five thousand kilometers may be confined to, and heat, the middle chromospheric network. Other solutions to the model indicate that magnetic elements with horizontal spatial extents of about ten thousand to thirty thousand kilometers may span and heat the middle chromospheric internetwork, and may be the building blocks of the chromospheric magnetic canopy. It is suggested that the middle chromosphere is highly structured over a wide range of spatial scales determined by the properties of these magnetic elements, and stronger, larger scale potential fields.

Key words: Sun: chromosphere – Sun: magnetic fields – MHD

1. Introduction

This paper continues the development of a series of magnetohydrodynamic (MHD) models which provide support for the proposition that a major source of heating for the solar middle chromosphere is resistive dissipation of large scale electric currents flowing orthogonal to the magnetic field in weakly ionized, closed magnetic loops called magnetic elements. The currents are large scale in that their scale heights are hundreds of kilometers in the network, and thousands of kilometers in the internetwork. The basic heating mechanism is introduced by Goodman (1995) in the context of a global model which is replaced by a more realistic, local model in Goodman (1996). The model presented here generalizes that presented in Goodman (1996) by including a driving mechanism in the form of a two dimensional velocity field. The component of the velocity field orthogonal to the magnetic field generates a convection electric field which drives a proton current that heats the gas by resistive dissipation described by the Pedersen resistivity for current flow orthogonal to the magnetic field in a weakly ionized gas. This paper introduces a key element of the proposed heating mechanism, a convection generated driving electric field. The model is steady state, and so does not include effects of time dependent processes such as wave generation, propagation, and dissipation on middle chromospheric heating. It is proposed that in the real, dynamic chromosphere time dependent convection electric fields drive currents orthogonal to the magnetic field, and that resistive dissipation of these currents provides an important source of heating.

A basic component of the proposed heating mechanism is the assumption that the hydrogen gas throughout most of the middle chromosphere is weakly ionized to a degree which implies that the appropriate electrical conductivity tensor is that for a weakly ionized gas as derived by Chapman & Cowling (1970). Standard one dimensional, semi - empirical, hydrostatic models of the solar chromosphere and transition region (Anderson & Athay 1989a,b; Maltby et al. 1986; Avrett 1984; Athay 1981; Vernazza et al. 1981, hereafter VAL) predict that the neutral hydrogen number density is $\sim 10 - 10^2$ times greater than the proton and electron number densities throughout most of the middle chromosphere. In the lower regions of the solar atmosphere the degree of ionization predicted by these models may be too large by several orders of magnitude (Feldman 1993). Based

Send offprint requests to: Michael L. Goodman

on this evidence it is assumed here that the degree of ionization is small enough to justify describing electrical conduction by the electrical conductivity tensor for a weakly ionized gas.

The internetwork middle chromosphere may be co - spatial with a magnetic canopy, thought to consist of a layer of mainly horizontal magnetic field lines filling the region between the temperature minimum and the upper chromosphere, and covering the area over the interior of supergranules (Solanki et al. 1994). It is proposed here that solutions to the model having magnetic elements with horizontal spatial scales comparable to a large fraction of an average supergranule diameter of $\sim 3\times10^4$ km describe magnetic loops which span and heat the middle chromospheric internetwork, and are the building blocks of the magnetic canopy. It is also proposed that solutions to the model having magnetic elements with smaller horizontal spatial scales of $1000-5000$ km describe magnetic loops which are confined to, and heat, the middle chromospheric network. Both classes of magnetic elements have a central region of almost vertical magnetic field where the field strength is a maximum. The central regions of both classes of elements may be based in the chromospheric network and be the continuation from the photosphere of the fields of strong, vertical magnetic flux tubes concentrated at the boundaries of supergranules. These flux tubes have subarcsecond radii and field strengths of $\sim 1-2$ kG (Lin 1995; Solanki 1993; Schussler 1992; Zwann 1987), and are observed to have a high degree of spatial proximity with the chromospheric network down to a spatial resolution of $\sim 1''$ (Muller 1985). In the quiet Sun (i.e. outside of active regions and sunspots) the most intense chromospheric heating takes place in the network within a few arcseconds of regions of strong magnetic field (Zwann 1981). Solutions to the model presented here suggest that middle chromospheric heating takes place inside magnetic structures, and that the regions of maximum heating are horizontally displaced from the regions where the magnetic field is strongest and mainly vertical.

The model is restricted to the middle chromosphere including network and internetwork regions. However, there is strong evidence for magnetic field related heating in the lower chromospheric network and internetwork. Recent measurements of internetwork magnetic fields in the photosphere indicate the presence of magnetic flux tubes with an average field strength of 500 G (Lin 1995; also see Keller et al. 1994 for a review of observations up to 1993). Since the photosphere is the lower boundary of the chromosphere the presence of these strong internetwork fields in the photosphere suggests that they play a role in lower chromospheric heating in the internetwork. A causal connection between internetwork bright points and magnetic fields is suggested by Sivaraman & Livingston (1982), and Kalkofen (1996), and differs from the proposal that heating of the lower internetwork chromosphere is due to the purely hydrodynamic mechanism of the compression due to, and the viscous dissipation of, acoustic shock waves (Carlsson & Stein 1995, 1994, 1992; Rammacher & Ulmschneider 1992; Rutten & Uitenbroek 1991; Kalkofen 1989; Cram & Damé 1983). Title & Berger (1996) present observational evidence of a close spatial proximity of photospheric bright points and magnetic field concentrations in active regions and supergranulation network. It appears that the magnetic field plays an important role in heating the lower chromosphere wherever it exceeds several hundred gauss. The relatively weak field region of the lower chromosphere, which appears to cover most of the interior of supergranules, may be heated by a primarily hydrodynamic, as opposed to MHD, mechanism.

2. Basic equations

2.1. General remarks

Cylindrical coordinates (R,θ,z) are used where R measures horizontal distance parallel to the photosphere and z measures distance from the center of the Sun along a radial line. All quantities are assumed to be independent of θ and time.

The Pedersen resistivity for protons is used in Ohm's law (1) to describe resistive heating of the weakly ionized hydrogen gas. In a weakly ionized gas consisting of protons, electrons, and neutrals, the proton Pedersen conductivity is $(m_{\rm p}/m_{\rm e})^{1/2}(\sim 43)$ times larger than the electron Pedersen conductivity when the protons are magnetized, defined by the condition $(\omega_{\rm p}\tau_{\rm pn})^2 \gg 1$ where $\omega_{\rm p}$ and $\tau_{\rm pn}$ are the proton cyclotron frequency and proton - neutral collision time. In this case the protons carry most of the Pedersen current (Chapman & Cowling 1970). It is assumed that the protons are magnetized, and this is verified for the solutions discussed in Sect. 5. The Pedersen resistivity is assumed to be constant to simplify the model. Its value is determined by the inputs to the model.

The interaction of protons with neutral hydrogen is taken into account in the neutral hydrogen momentum Eqs. (8) and (9) through the Lorentz force, and in Ohm's law (1) through the proton resistivity. The Lorentz force on the protons is transmitted to neutral hydrogen through proton - hydrogen collisions. The number density of the most abundant ions in the middle chromosphere is estimated to be several orders of magnitude smaller than the proton number density (VAL; Anderson 1989), so they do not make the dominant contribution to the Lorentz force or Pedersen conductivity, although they emit most of the net radiation from the chromosphere. An estimate of the ratio of the proton and ion Pedersen conductivities is given by Goodman (1995).

It is assumed that $B_\theta = 0$. This assumption, together with the assumption $\partial/\partial\theta = 0$, implies through Ampères law that $J_z = J_R = 0$, so there is no current parallel to $\boldsymbol{B}$. These assumptions are made in order to construct a simple model that isolates the effect of resistive dissipation of current flowing orthogonal to a magnetic loop in a weakly ionized plasma.

The hydrogen flow velocity $\boldsymbol{V}$ is assumed to be independent of z to simplify the model. It is also assumed that $V_\theta = 0$ to simplify the model. Then $\boldsymbol{B}$ and $\boldsymbol{V}$ are restricted to the R,z plane, which is a simple configuration allowing for the generation of a convection electric field $(\boldsymbol{V}\times\boldsymbol{B})/c$ which drives the current density J_θ orthogonal to $\boldsymbol{B}$.

The energy equation (6) describes the energy conversion process proposed to account for a major part of the net radiative

loss of the middle chromosphere. It is assumed that the primary heating mechanism is resistive dissipation, and that the primary cooling mechanism is radiation. It is unlikely that thermal conduction is important in heating or cooling the middle chromosphere for the following reason. Semi - empirical models of the quiet sub - coronal solar atmosphere (VAL; Anderson & Athay 1989a) indicate that the temperature range in the middle chromosphere is $\sim 6000 - 8000$ K. According to these models the height range of the middle chromosphere is several thousand kilometers. The average vertical temperature gradient suggested by these models is then ~ 1 K-km^{-1}. The temperature gradient in the horizontal direction is unlikely to be many orders of magnitude greater than this. In order that thermal conduction be important for middle chromospheric heating or cooling it is necessary that the thermal energy flux be comparable to the net radiative loss $F \sim 10^7$ ergs-cm^{-2}-sec^{-1}. A lower limit on the temperature gradient necessary to drive a thermal flux of this magnitude may be estimated as follows. The middle chromosphere is weakly ionized, and the thermal conductivity of a fully ionized gas is much greater than that of a neutral gas. The thermal conductivity of the middle chromosphere lies between these two extreme values. For a temperature of 10^4 K and a Coulomb logarithm of 10, the electron thermal conductivity parallel to the magnetic field in a fully ionized hydrogen plasma is $\sim 2.4 \times 10^4$ ergs-K^{-1}-cm^{-1}-sec^{-1}. Setting the thermal flux equal to F implies a temperature gradient of $\sim 4.2 \times 10^7$ K-km^{-1} which is many orders of magnitude larger than may reasonably be expected to exist in the middle chromosphere.

The temperature is assumed to be constant, and is an input to the model. Since semi - empirical models indicate that the average temperature varies slowly with height in the middle chromosphere, and since thermal conduction is probably not important for energy balance in the middle chromosphere, this assumption is reasonable as a first approximation. However, this assumption should eventually be relaxed in order to compare the distribution of the heating rate in the magnetic loop with that of a temperature computed self consistently.

The geometry of the magnetic field is specified and discussed in detail in Sect. 3.2. The field has the form of a magnetic element, which has a non - zero curl and a loop like geometry, plus a potential field. The maximum magnitude of the magnetic element field is an input to the model, and that of the potential field is computed as a function of the inputs to the model. The base of the element is assumed to be at the base of the middle chromosphere. An example of these fields is shown in Figs. 1 and 2. The corresponding total magnetic field is shown in Fig. 3. All of the heating takes place in the magnetic element. In all cases studied the magnetic element field is much weaker than the potential field.

2.2. Maxwell's equations

Let η be the resistivity defined as the inverse of the high magnetic field limit of the Pedersen conductivity for protons flowing orthogonal to the magnetic field in a weakly ionized plasma. The Pedersen conductivity is derived by Chapman & Cowling (1970).

Ohm's law

$$\boldsymbol{E} + \frac{(\boldsymbol{V} \times \boldsymbol{B})}{c} = \eta J_\theta \hat{\theta} \tag{1}$$

and $\nabla \times \boldsymbol{E} = 0$, when combined with the assumptions that $V_\theta = B_\theta = 0$, and the requirement that E_θ be finite at $R = 0$, reduce to $\boldsymbol{E} = 0$ and

$$\frac{(V_z B_R - V_R B_z)}{c} = \eta J_\theta. \tag{2}$$

Here

$$\eta = \frac{B^2}{c^2 \sigma (m_\mathrm{p} k_\mathrm{B} T)^{1/2} n_\mathrm{p} n_\mathrm{H}} \tag{3}$$

and $B, \sigma, m_\mathrm{p}, k_\mathrm{B}, T, n_\mathrm{p}, n_\mathrm{H}$ and c are the magnitude of $\boldsymbol{B}$, proton - hydrogen scattering cross section, proton mass, Boltzmann's constant, temperature, proton number density, hydrogen number density, and the speed of light. The cross section σ is assumed to be constant and equal to 5×10^{-15} cm^2 (Book 1990). The constant value of η used to generate a particular solution is determined by substituting $B(R = 0, z = z_0), n_\mathrm{p}(R = 0, z = z_0)$, and $n_\mathrm{H}(R = 0, z = z_0)$ into Eq. (3) along with the assumed constant value of T. Here $z - z_0$ measures height above the base of the magnetic element, and the center of the magnetic element is at $R = 0, z = z_0$.

The result that the total electric field $\boldsymbol{E}$ is zero, together with Eq. (2), implies that the current is driven entirely by the convection electric field $\boldsymbol{E}_\mathrm{c} \equiv (\boldsymbol{V} \times \boldsymbol{B})/c$ generated by the flow of hydrogen gas across the magnetic field. The small fraction of ionized gas in the middle chromosphere is entrained in the hydrogen flow across the magnetic field and experiences the convection electric field.

Ampère's law reduces to

$$\frac{\partial B_R}{\partial z} - \frac{\partial B_z}{\partial R} = \frac{4\pi J_\theta}{c} \tag{4}$$

which is used to calculate J_θ.

The divergence free condition is

$$\frac{1}{R}\frac{\partial (R B_R)}{\partial R} + \frac{\partial B_z}{\partial z} = 0. \tag{5}$$

2.3. Energy balance

Let $F(R)$ be the net radiation flux from the middle chromosphere. The radiation flux is assumed to be equal to the height integrated resistive heating rate per unit volume. The energy equation is then given by

$$F(R) = \int_{z_0}^{\infty} \eta J_\theta^2 \, dz \tag{6}$$

where the upper limit of integration may be extended to infinity due to the exponentially rapid decrease of the current density with height.

2.4. Mass conservation

The equation of mass conservation is

$$\frac{1}{R}\frac{\partial(R\rho V_R)}{\partial R} + V_z\frac{\partial \rho}{\partial z} = 0 \tag{7}$$

where $\rho = m_{\rm p} n_{\rm H}$ is the hydrogen mass density.

2.5. Momentum conservation

The momentum conservation equation reduces to

$$\rho V_R \frac{{\rm d}V_R}{{\rm d}R} + \frac{\partial p}{\partial R} = \frac{J_\theta B_z}{c} \tag{8}$$

$$\rho V_R \frac{{\rm d}V_z}{{\rm d}R} + \frac{\partial p}{\partial z} = -\frac{J_\theta B_R}{c} - \rho g_\odot \tag{9}$$

where p is the hydrogen gas pressure and $g_\odot = 2.74 \times 10^4$ cm-sec^{-2} is the gravitational acceleration at the photosphere. Over the height range of the middle chromosphere, which for the examples considered in Sect. 5 is at most $\sim 4.5 \times 10^4$ km, the fractional variation of z from $R_\odot$ is $\sim 6\%$, while the density ρ decreases exponentially with height with a scale height ranging from 350 to 9000 km. Then the variation in the gravitational force term is almost completely determined by the variation in density, so that the gravitational acceleration may be regarded as constant with negligible error.

3. Assumed form of solution

3.1. Height dependence

Inspection of the momentum conservation Eqs. (8) - (9) shows that an exact and reasonable solution for the height dependence of the density, pressure, and magnetic field is given by

$$\rho(R,z) = \rho_0(R) e^{-(z-z_0)/L} \tag{10}$$

$$p(R,z) = p_0(R) {\rm e}^{-(z-z_0)/L} \tag{11}$$

$$B_R(R,z) = b_R(R) {\rm e}^{-(z-z_0)/2L} \tag{12}$$

$$B_z(R,z) = b_z(R) {\rm e}^{-(z-z_0)/2L} \tag{13}$$

where L is the pressure scale height that is assumed to be constant, and is an input to the model. When this form of the solution is substituted into the basic equations the exponential factor cancels out after performing the required differentiations with respect to z. This simplifies the model since the resulting equations, which must be solved numerically, only depend on R.

3.2. Magnetic field

The magnetic field is specified as the sum of a loop shaped, non - potential field, called a magnetic element, and a potential field. It follows that the current density and resistive heating are confined to the region occupied by the magnetic element. Let $b_R = b_{1R} + b_{2R}$, and $b_z = b_{1z} + b_{2z}$, where the subscripts 1 and 2 label the magnetic element and potential magnetic field.

The equations for the R and z components of the magnetic field of the magnetic element, and its associated current density, are derived by Goodman (1996), and imply that

$$b_{1R} = \frac{B_1 R_B}{2x^*\, L} J_1\left(\frac{x^* R}{R_B}\right) \tag{14}$$

$$b_{1z} = B_1 J_0\left(\frac{x^* R}{R_B}\right) \tag{15}$$

$$J_\theta(R, z_0) = \frac{cB_1 x^*}{4\pi R_B}\left(1 - \left(\frac{R_B}{2x^*\, L}\right)^2\right) J_1\left(\frac{x^* R}{R_B}\right) \tag{16}$$

with $R \le R_B$. Here R_B is the radial distance from $R = 0$ to the point at which the field returns to the base of the middle chromosphere, and is called the radius of the magnetic element. J_0 and J_1 are the Bessel functions of zero and first order, and $x^* \sim 3.832$ is the first zero of $J_1(x)$. B_1 is the maximum magnitude of the field, and is an input to the model. A two dimensional plot of this field is presented in Fig. 1 where $R_B = 5000$ km.

The assumed height dependence, and the divergence and curl free conditions which must be satisfied by the potential magnetic field imply that

$$b_{2R} = B_2\, J_1\left(\frac{R}{2L}\right) \tag{17}$$

$$b_{2z} = B_2\, J_0\left(\frac{R}{2L}\right) \tag{18}$$

where B_2 is the maximum magnitude of the potential field, and is determined from the energy equation (6) in the following way. Substitute Eq. (16) for the current density into the energy equation, use Eq. (3) to express η in the energy equation in terms of the boundary values $B(0, z_0), n_{\rm H}(0, z_0),$ and $n_{\rm p}(0, z_0)$, and carry out the indicated integration. Then average the resulting equation, which only depends on R, over the circular area $\pi R_{\rm B}^2$ of the base of the magnetic element, and solve for B_2 to obtain

$$B_2 = \pm\left\{\frac{\Gamma_2}{\Gamma_1}\right\}^{1/2} \frac{1}{B_1} - B_1 \tag{19}$$

where

$$\Gamma_1 = \left(\frac{e}{m_{\rm p} c}\right)^2 \tag{20}$$

$$\Gamma_2 = \frac{< F > \sigma n_{\rm p0} n_{\rm H0}}{.162L}\left(\frac{k_{\rm B} T}{{m_{\rm p}}^3}\right)^{1/2} \times \left(\frac{4\pi R_{\rm B} e}{x^* c}\frac{(2x^* L)^2}{((2x^* L)^2 - {R_{\rm B}}^2)}\right)^2. \tag{21}$$

Here $n_{\rm H0} = n_{\rm H}(0, z_0)$, $n_{\rm p0} = n_{\rm p}(0, z_0)$, and $< F >$, which is an input to the model, is the average of the radiation flux $F(R)$ over the area of the base of the magnetic element. It is assumed that $B_1 \ge 0$. In this case solutions are found only for the choice of the positive root in Eq. (19). A two dimensional plot of the potential field is presented in Fig. 2 where $R_{\rm B} = 5000$ km.

The complete set of inputs, including boundary conditions and constraints necessary to determine the solution to the model

are identified by examining the equations for numerical solution presented in Sect. 4. These equations are obtained by rewriting the basic equations as two groups; a set of differential equations, and a set of algebraic equations. Once these differential equations are solved, all other profiles are determined algebraically in terms of their solution.

4. Equations for numerical solution

Normalize R to L, and define $r = R/L$. The differential equations that must be solved to determine the equilibrium state are,

$$\frac{\mathrm{d}V_R}{\mathrm{d}r} = \frac{V_R}{2}\left[\frac{b^2}{b_R b_z} + \frac{b_{1R}(\alpha^2-1)}{b_z} - \frac{2}{r}\right] - \frac{c^2\eta(\alpha^2-1)}{16\pi L b_R b_z}\left[b_{2R}b_{1z} - b_{1R}b_{2z}\right] + \frac{b_R}{\rho_0 V_R b_z}\left[p_0 - \frac{(\alpha^2-1)b_{1R}b_R}{8\pi} - L\rho_0 g_\odot\right] \quad (22)$$

$$\frac{\mathrm{d}\rho_0}{\mathrm{d}r} = \rho_0\left[-\frac{1}{V_R}\frac{dV_R}{dr} - \frac{1}{r} + \frac{b_z}{b_R} + \frac{c^2\eta(\alpha^2-1)}{8\pi L}\frac{b_{1R}}{V_R b_R}\right] \quad (23)$$

$$\frac{\mathrm{d}p_0}{\mathrm{d}r} = -\rho_0 V_R\frac{dV_R}{dr} + \frac{(\alpha^2-1)b_{1R}b_z}{8\pi} \quad (24)$$

where $\alpha = 2x^*L/R_\mathrm{B} \sim 7.66L/R_\mathrm{B}$, and Eq. (22) is to be used for $\mathrm{d}V_R/\mathrm{d}r$ in Eqs. (23) and (24).

By examining the behavior of Eqs. (22) - (24) near $R = 0$ it is found that the following boundary conditions must be satisfied at $R = 0$,

$$V_R(0) = 0 \quad (25)$$

$$p_0(0) = L\rho_0(0)g_\odot. \quad (26)$$

It is expected that the pressure increases with R near $R = 0$. In order that the pressure profile exhibit this behavior it is found to be necessary that $\mathrm{d}^2p/\mathrm{d}R^2 > 0$ at $R = 0$ which, from an analytic expansion of p in powers of R near $R = 0$, implies that $\alpha > 1$ which is equivalent to the condition that $R_\mathrm{B} < 2x^*L \sim 7.66L$. This necessary condition is also found to be sufficient in that all numerical solutions for the pressure generated with this condition enforced exhibit the desired behavior. No solutions are found when the condition $R_\mathrm{B} < 2x^*L$ is not satisfied. For a given scale height this condition places an upper limit on the baseline radius R_B of the magnetic element in which the resistive heating takes place. In practice it is found that R_B must be significantly less than this upper limit in order for a solution to exist.

Eqs. (22) - (24) also imply that the following additional boundary conditions must be satisfied:

$$\left.\frac{\mathrm{d}V_R}{\mathrm{d}R}\right|_{R=0} = -\frac{c^2\eta(\alpha^2-1)B_1}{16\pi L^2(B_1+B_2)} < 0 \quad (27)$$

$$\left.\frac{\mathrm{d}\rho}{\mathrm{d}R}\right|_{R=0} = 0 \quad (28)$$

$$\left.\frac{\mathrm{d}p}{\mathrm{d}R}\right|_{R=0} = 0. \quad (29)$$

For the given form of the magnetic field, the inputs to the model that uniquely determine the solution are $n_{\mathrm{H}0}, n_{\mathrm{p}0}, L, <F>, \sigma, R_\mathrm{B},$ and B_1. No information about the velocity field is specified as an input. The velocity field is computed self consistently once the inputs just indicated are given.

Once B_2 and V_R are determined, the z component of the velocity is given by

$$V_z(R) = \frac{1}{b_R}\left(V_R b_z + \frac{c^2\eta(\alpha^2-1)b_{1R}}{8\pi L}\right) \quad (30)$$

where

$$V_z(0) = -\frac{c^2\eta(\alpha^2-1)B_1}{8\pi L(B_1+B_2)} < 0, \quad (31)$$

indicating that the hydrogen flows downward towards the photosphere in the region where the magnetic field is strongest and mainly vertical. Only solutions with a downward vertical component of velocity are found.

The heating rate per unit volume is ηJ_θ^2, and is computed using Eqs. (3) and (16) with $B = B_1 + B_2, n_\mathrm{p} = n_{\mathrm{p}0},$ and $n_\mathrm{H} = n_{\mathrm{H}0}$ in Eq. (3). The heating rate per unit mass is

$$q = \frac{\eta J_\theta^2}{m_\mathrm{p} n_\mathrm{H}} \quad (32)$$

The value of q in the middle chromosphere, as computed by Anderson & Athay (1989a), is used as a guide for generating solutions to the model, as discussed in Sect. 5.1.

5. Particular solutions

5.1. General remarks

Four solutions, labeled a - d, are presented in Figs. 1 - 13. All plots except the vector field plots are for $z = z_0$, and hence present profiles across the base of the magnetic element, assumed to be at the base of the middle chromosphere. Scale heights and average values of quantities are indicated in the figure captions. The average values are computed over the base area πR_B^2 of the magnetic element. For all solutions the inputs $T = 7000$ K, $< F >= 2 \times 10^7$ ergs-cm^{-2}-sec^{-1}, and $\sigma = 5 \times 10^{-15}$ cm^2 are used. The remaining inputs for solutions a - d are $(n_{\mathrm{H}0}(\mathrm{cm}^{-3}), n_{\mathrm{p}0}(\mathrm{cm}^{-3}), L(\mathrm{km}), R_\mathrm{B}(\mathrm{km}), B_1(\mathrm{G})) = (4\times10^{13}, 10^8, 350, 1000, 19)$, $(10^{13}, 10^7, 1500, 5000, 11)$, $(6\times10^{12}, 10^7, 3000, 10^4, 9)$, and $(1.5\times10^{12}, 10^7, 9000, 3\times10^4, 8)$. The solutions are chosen to demonstrate that magnetic structures with horizontal length scales ranging from $\sim$ 1000 to $\sim 3 \times 10^4$ km may be heated at the required rate of 2×10^7 ergs-cm^{-2}-sec^{-1} by the proposed heating mechanism, and that the predicted properties of the plasma in these structures are for the most part reasonable. The smaller magnetic elements may be confined to, and heat, the middle chromospheric network. The largest structures with $R_\mathrm{B} \sim 3 \times 10^4$ km may be based in the network, arch over a supergranule, and form the magnetic canopy in the middle chromospheric internetwork. It is likely that the chromosphere is highly structured over a wide range of

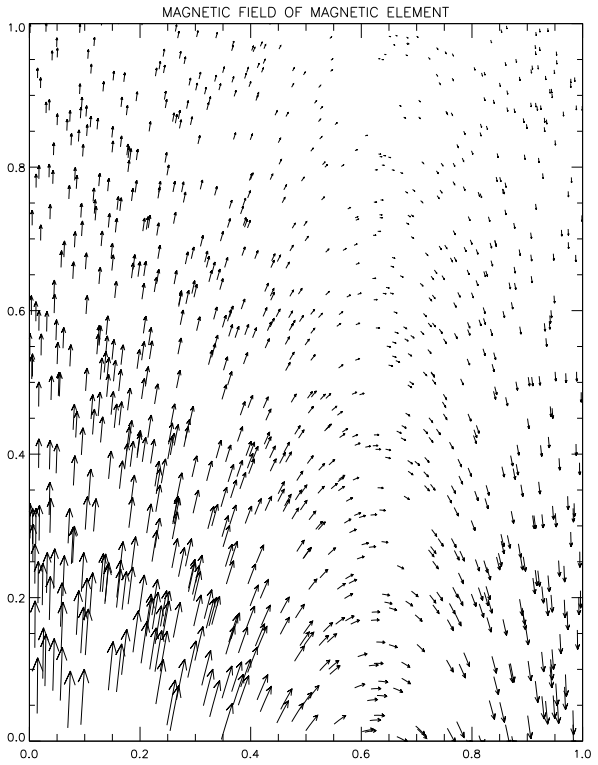

Fig. 1. Magnetic field vectors of the magnetic element of solution b. The horizontal axis measures normalized distance $R/5000$ km parallel to the photosphere from the center of the element at R = 0. The vertical axis measures normalized height $(z - z_0)/6000$ km above the base of the middle chromosphere. The length of the vectors is proportional to the field strength. The magnetic field of the elements has the same basic geometry for all solutions.

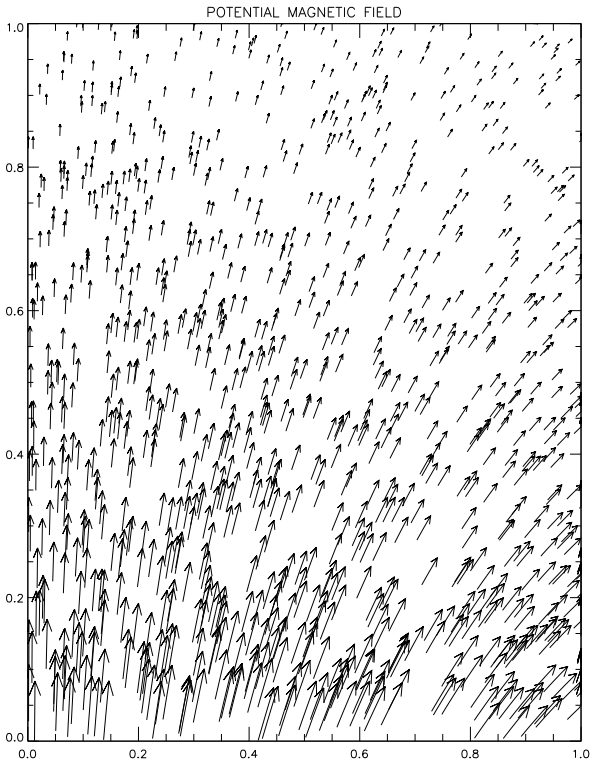

Fig. 2. Magnetic field vectors for the potential magnetic field of solution b. The axis definitions and normalizations are the same as for Fig. 1. The potential magnetic field has the same basic geometry for all solutions.

horizontal spatial scales determined by three dimensional magnetic elements of varying size and magnetic field strength.

The guidelines used to generate solutions a - d take the form of requirements at the base of the magnetic element, and are as follows. The maximum magnetic field strength is restricted to being less than 200 G since this is a reasonable upper limit for the maximum field strength at the base of the middle chromosphere. The average value of the pressure is required to be $\sim$ 100 dynes-cm^{-2}. The average value of the hydrogen density is restricted to be in the range of $\sim 10^{12} - 10^{14}$ cm^{-3}. The average value of the heating rate per unit mass is restricted to being in the range of one to two times the value of 4.5×10^9 ergs-g^{-1}-sec^{-1} predicted by the model of Anderson & Athay (1989a). The values of the model input parameters are adjusted until solutions satisfying these criteria are obtained. The average values of pressure and hydrogen density are chosen to be comparable to the corresponding values predicted for the middle chromosphere by standard one dimensional models (Anderson & Athay 1989a, Maltby et al. 1986; Avrett 1984; VAL; Athay 1981).

5.2. Detailed discussion

5.2.1. Magnetic field

Fig. 1 shows the magnetic field geometry for the magnetic element having $R_{\rm B}$ = 5000 km, corresponding to solution b. The field strength is a maximum at R = 0. The magnetic elements of all solutions have the same basic geometry.

Fig. 2 shows the geometry of the potential magnetic field for solution b. The field strength is a maximum at R = 0. The potential field of all solutions has the same basic geometry. The rate at which the field lines diverge, and the rate at which the field strength decreases with R is much slower than for the magnetic element. From Eqs. (17) - (18) the horizontal length scale associated with this field is estimated to be $2Lx^*(\sim 7.66L)$ since this is the value of $R > 0$ at which the potential field returns to the height of the base of the magnetic element. Since L = 1500 km for solution b the horizontal scale of the potential field is $\sim 1.2 \times 10^4$ km which is $\sim 2.3R_{\rm B}$. For solutions a, c, and d the horizontal scales of the potential fields are $\sim 2.7 \times 10^3, 2.3 \times 10^4,$ and 6.9×10^4 km which may be compared with the corresponding values of $R_{\rm B}$ given by $10^3, 10^4,$ and 3×10^4 km. For solutions a - d the maximum strengths of the potential fields are $170.2, 121.9, 169.0,$ and 165.5 G. These may be compared with the maximum field strengths of the corresponding magnetic element fields of $19, 11, 9,$ and 8 G. Hence the magnetic field configuration for all solutions consists of a mag-

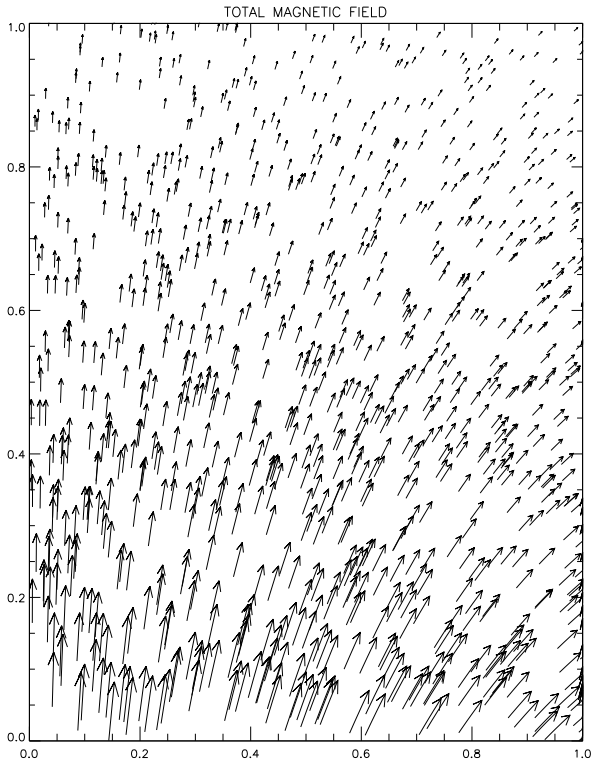

Fig. 3. Magnetic field vectors for the total magnetic field of solution b. The axis definitions and normalizations are the same as for Fig. 1. The total magnetic field has the same basic geometry for all solutions.

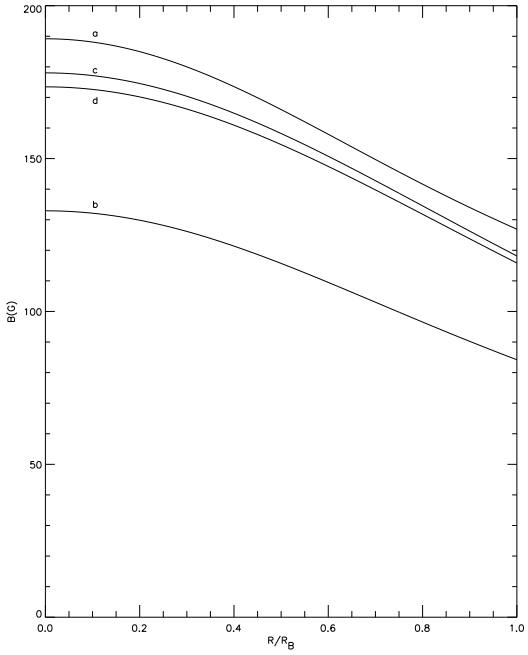

Fig. 4. Magnitude of the total magnetic field vs. $R/R_{\rm B}$ for $(z - z_0)$ = 0. The scale height of B for solutions a - d is 700, 3000, 6000, and 18,000 km. The average values of B for solutions a - d are 152.0, 104.5, 144.1, and 141.0 G.

netic element embedded in a much stronger potential field that has a horizontal scale size $\sim 2 - 3$ times larger than that of the magnetic element. The total magnetic field for solution b is shown in Fig. 3 where the magnetic element is no longer visible. If magnetic structures similar to those generated by the model exist in the middle chromosphere, then unless such fields are measured with sufficiently high accuracy, the weak field component corresponding to the magnetic element is undetectable, and the measured field appears to be a potential field, although the structure radiates due to the resistive heating of the magnetic element. The magnetic element has a closed loop geometry so that one may observe radiating loops in regions where the magnetic field appears to be potential. The loop geometry, and the fact that the heating is confined within the loop, are consistent with observations and semi - empirical models which indicate that bright magnetic loops are present throughout the network chromosphere, extending from the temperature minimum region up to the lower transition region (Karovska & Habbal 1991; Foing et al. 1986). It appears that, at least in the network, almost all emitting chromospheric magnetic structures are closed and have a looplike geometry.

Fig. 4 shows the magnitude of the total magnetic field. In the temperature minimum region in the network, bright magnetic loops, for which the line of sight field strength is proportional to the brightness temperature, and is as large as $\sim$ 150 G, appear to exist (Cook & Ewing 1990; Foing et al. 1986). This field strength is close to the maximum field strengths in the model solutions a - d. The maximum field strengths for these solutions are imagined to occur at the base of the middle chromosphere, which is just above the temperature minimum.

The largest magnetic elements, corresponding to solutions c and d, are meant to represent basic elements of the chromospheric magnetic canopy which may be co - spatial with the middle chromosphere in the internetwork. The canopy is believed to consist of a mainly horizontal magnetic field covering the internetwork chromosphere over quiet and active regions, and beginning just above the temperature minimum (Faurobert - Scholl 1994, 1992). The canopy presumably extends upwards at least to the base of the transition region. The magnetic field at the lower boundary of the canopy appears to have a random horizontal component of $\sim$ 30 G that is related to the weak turbulent component of the underlying photospheric magnetic field (Faurobert - Scholl et al. 1995; Faurobert - Scholl 1994, 1993). The central regions of the canopy elements represented by solutions c and d, where the magnetic field is strongest and mainly vertical, are interpreted as the extension into the chromosphere of flux tubes based in the photospheric network which flare out with increasing height, spanning the internetwork region and forming the canopy. This interpretation is consistent with the model results of Briand & Solanki (1995) and Solanki & Steiner (1990) which indicate that in the lower network chromosphere the temperature rise begins at a substantially lower height in magnetic elements than in the relatively cool surrounding plasma, and that the heating of the elements generates a pressure that is higher than in the surrounding plasma causing

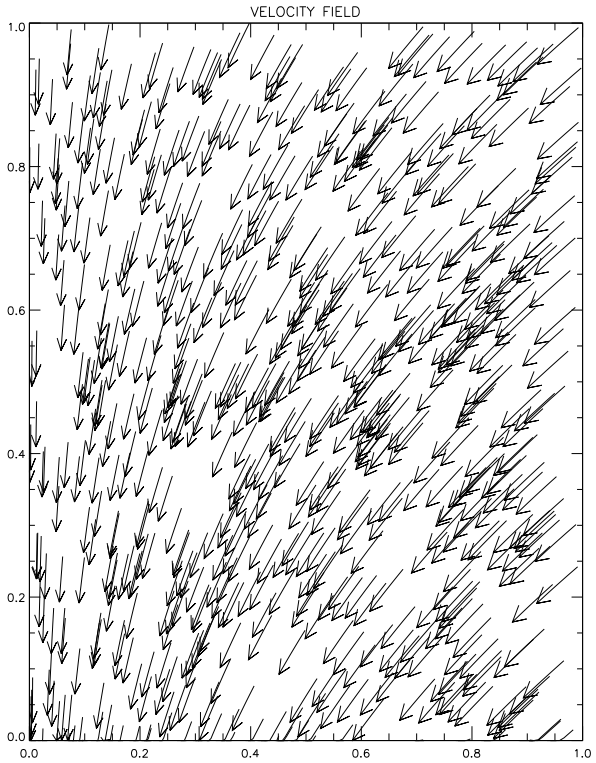

Fig. 5. Velocity vectors for the velocity field of solution b. The axis definitions and normalizations are the same as for Fig. 1. The length of the vectors is proportional to the flow speed. The velocity field is independent of height, and has the same basic geometry for all solutions.

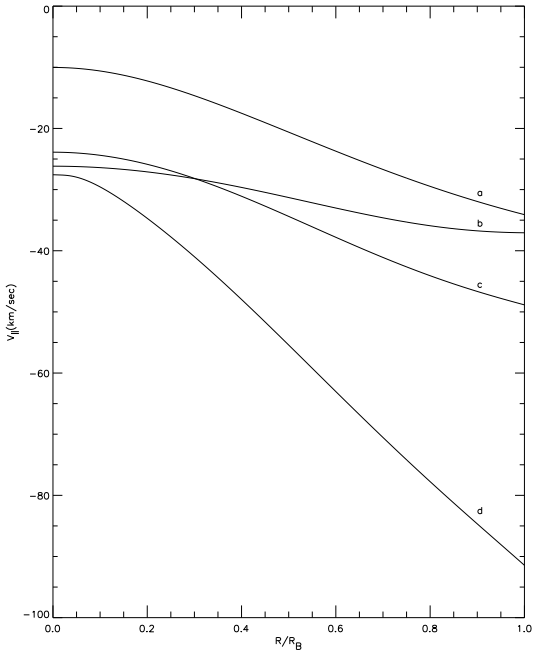

Fig. 6. Velocity parallel to $\boldsymbol{B}$ vs. $R/R_{\rm B}$. The average values of $V_{\|}$ for solutions a - d are -25.5, -33.7, -39.7, and -67.9 km-sec^{-1}.

the field lines to expand rapidly outwards forming a magnetic canopy that fills the middle and upper chromosphere.

5.2.2. Hydrogen velocity field, electric field and current density

Fig. 5 shows the geometry of the velocity field for solution b. Figs. 6 and 7 show the velocity field decomposed into components parallel and perpendicular to $\boldsymbol{B}$. The velocity field has the same basic geometry for all solutions. All of the solutions exhibit downflow towards the region, near R = 0, where $\boldsymbol{B}$ is strongest and mainly vertical. The downflow is weakest in this region. Larger magnetic structures have larger flow speeds. The velocity is nearly parallel to $\boldsymbol{B}$. The relatively small component of velocity perpendicular to $\boldsymbol{B}$ is a maximum in the midpoint region of the magnetic element, near $R = R_{\rm B}/2$, where the magnetic field is mainly horizontal, and the heating rates, shown in Figs. 10 and 11, are largest. This velocity component generates a convection electric field that drives the current which heats the weakly ionized middle chromospheric gas through resistive dissipation. The current density is shown in Fig. 8. Larger magnetic elements have smaller current densities. The maximum current density is a few mA-m^{-2}. The convection electric field is shown in Fig. 9. The maximum value of $E_{c\theta}$ increases slowly with the size of the magnetic structure from $\sim$ 40 to $\sim$ 120 V-m^{-1}.

There do not appear to be any measurements of the electric field or current density in the quiet middle chromosphere. However, Chang & Schoenfeld (1991) present observational evidence for the existence of quasi - static electric fields as large as 10^4 V-m^{-1} in the quiet Sun photosphere. The electric field strengths computed by Chang & Schoenfeld (1991) are derived from measurements of the quadratic Stark effect. The electric field experienced by an atom undergoing Stark splitting is $\boldsymbol{E}+(\boldsymbol{V}\times\boldsymbol{B})/c$, and so includes the effect of convection. Electric field strengths in the photosphere are expected to be much larger than in the middle chromosphere since the photosphere is more weakly ionized than the middle chromosphere, and since the maximum magnetic field strengths in the photosphere are much greater than in the middle chromosphere. The electric field strengths for the model solutions a - d are consistent with this expectation.

Vertical, photospheric current densities in the range $15-80$ mA-m^{-2} are inferred to exist in active regions (Metcalf et al. 1994). These current densities are inferred to be parallel to $\boldsymbol{B}$. Current densities are expected to be larger in the photosphere than in the chromosphere due to the stronger fields and smaller scale heights in the photosphere. Then the current density computed in a model of the chromosphere is expected be much smaller than current densities in the photosphere. The current densities for the model solutions a - d are consistent with this expectation since the maximum current density for these solutions is five times smaller than the smallest current density computed by Metcalf et al. (1994), and throughout most of the region occupied by the magnetic loops used in the model the current density is at least an order of magnitude smaller than the smallest current density computed by Metcalf et al. (1994).

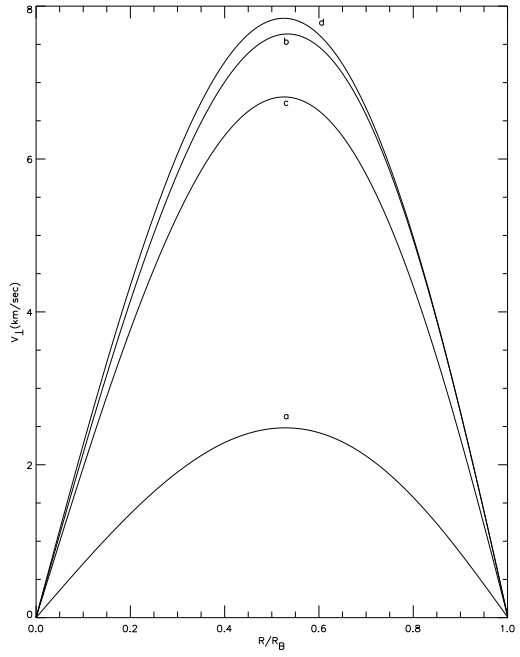

Fig. 7. Velocity perpendicular to $\boldsymbol{B}$ vs. $R/R_{\rm B}$. The average values of $V_\perp$ for solutions a - d are 1.6, 5.0, 4.4, and 5.1 km-sec^{-1}.

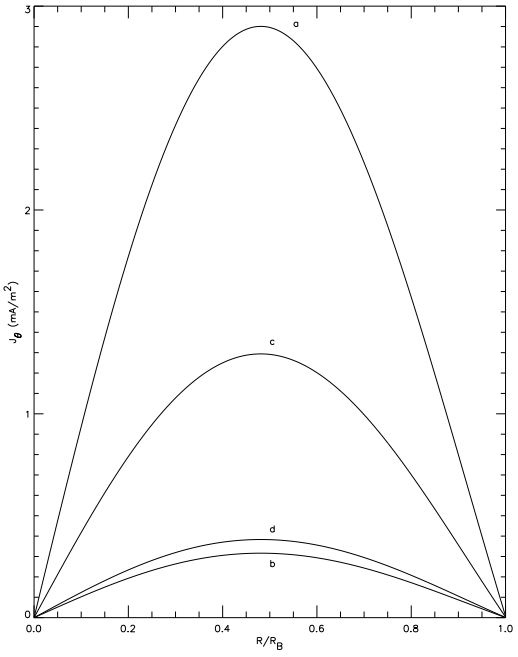

Fig. 8. Current density vs. $R/R_{\rm B}$ for $(z - z_0)$ = 0. (c) $J_\theta \times 10$. (d) $J_\theta \times 10$. Profiles (a) and (b) are unscaled. The scale height of J_θ is the same as for B in Fig. 4. The average values of J_θ for solutions a - d are 1.8, 0.2, 0.08, and 0.02 mA-m^{-2}.

The average flow speeds for solutions a - d are in the range of $\sim 26 - 68$ km-sec^{-1} and the maximum flow speeds are in the range of $\sim 35 - 90$ km-sec^{-1}. It appears that little is known about flow speeds in the middle chromosphere. More is known about flow speeds in the region extending from the base of the upper chromosphere ($T \sim 10^4$ K) to the lower transition region ($T \sim 10^5$ K). Since observation suggests that flow speeds tend to increase from the photosphere to the transition region, it is useful to compare flow speeds predicted by the model for the middle chromosphere with observed flow speeds in the upper chromosphere and lower transition region which form the upper boundary to the middle chromosphere. In the network, Hα observations indicate upflows and downflows ranging from $5 - 10$ km-sec^{-1} (Heinzel & Schmieder 1994). Steady flows of ~ 4 km-sec^{-1} on the scale of the supergranulation are observed to extend from the middle chromosphere ($6000 \leq T \leq 8000$ K) into the lower transition region (Gebbie et al. 1981; November et al. 1979). Steady flow speeds as high as ~ 20 km-sec^{-1} are observed in quiet and active regions near the base of the upper chromosphere, and in the lower transition region (Athay & Dere 1991; Athay et al. 1983, 1982). The direction of these flows appears to be downward towards the photosphere, and mainly parallel to the magnetic field, consistent with the flow patterns predicted by the model as indicated in Figs. 5 - 7. Chromospheric jets observed near the base of the quiet upper chromosphere reach speeds of ~ 20 km-sec^{-1} in the internetwork, and in the quiet lower transition region surge to speeds up to ~ 100 km-sec^{-1} (Dere et al. 1984, 1983). In enhanced network regions near the base of the upper chromosphere, jets are identified with spicules having flow speeds up to ~ 40 km-sec^{-1} with the flow velocity mainly parallel to the magnetic field (Suematsu et al. 1995; Grossmann-Doerth & Schmidt 1992; Hasan & Keil 1984). These observations indicate that the flow speeds predicted by the model are too high but are within factors of 5 and 10 of realistic flow speeds for the smaller ($R_{\rm B}$ = 1000, 5000 km) and larger ($R_{\rm B}$ = $10^4, 3 \times 10^4$ km) magnetic elements, respectively. A more general model which computes the two dimensional velocity self consistently as a function of R and z is needed to try to generate flow speeds in better agreement with observation.

In the photosphere, at the boundaries of supergranules, stationary downflows of $.1 - .5$ km-sec^{-1} are sometimes observed in regions adjacent to high field strength, small scale magnetic flux tubes, although the flows in most of these flux tubes are not stationary and have velocity amplitudes in the range of $.2 - 3$ km-sec^{-1} (Solanki 1993). The origin of these downflows is not known. The possibility that they are related to the faster downflows predicted by the model to exist higher in the atmosphere should be considered.

5.2.3. Heating rates, hydrogen density, and pressure

The heating rates per unit volume and per unit mass, ηJ_θ^2 and q, are shown in Figs. 10 and 11. The maximum value of ηJ_θ^2 steadily decreases by a factor of ~ 27 as $R_{\rm B}$ increases from 10^3 to 3×10^4 km. Although the largest elements have the smallest values of ηJ_θ^2, the maximum value of q does not vary by more than $\sim 24\%$ as $R_{\rm B}$ varies by a factor of 30. This is due to the behavior of the hydrogen density which is shown in Fig. 12 to decrease with increasing $R_{\rm B}$. Larger magnetic structures have

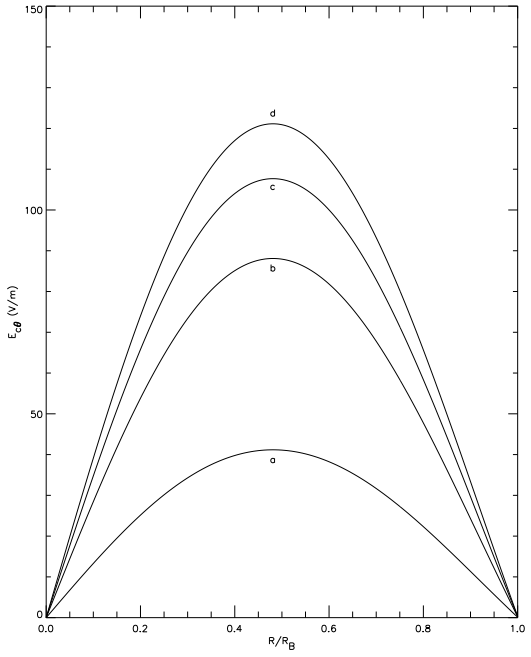

Fig. 9. Convection electric field vs. $R/R_{\rm B}$ for $(z - z_0)$ = 0. The scale height of $E_{c\theta}$ is the same as for B in Fig. 4. The average values of $E_{c\theta}$ for solutions a - d are 25.4, 54.3, 66.4, and 74.7 V-m^{-1}.

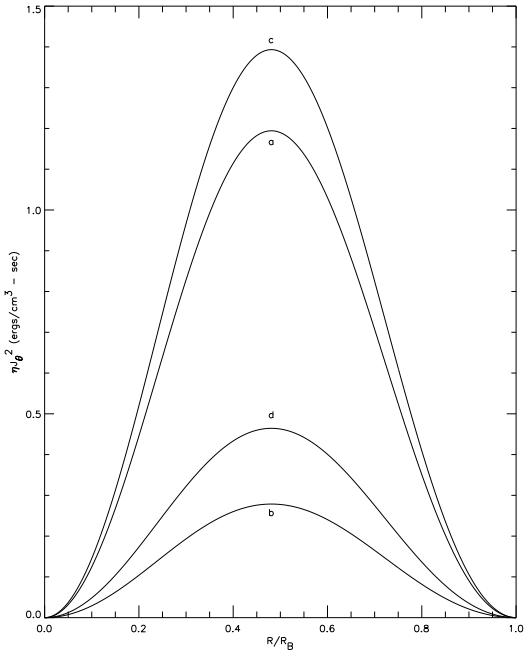

Fig. 10. Heating rate per unit volume vs. $R/R_{\rm B}$. (c) $\eta J_\theta^2 \times 10$. (d) $\eta J_\theta^2 \times 10$. Profiles (a) and (b) are unscaled. The scale height of $\eta {J_\theta}^2$ is the same as for the pressure in Fig. 13. The average values of $\eta {J_\theta}^2$ for solutions a - d are 0.57, 0.13, 0.07, and 0.02 ergs-cm^{-3}-sec^{-1}.

lower density. The profile of q is nearly invariant as $R_{\rm B}$ ranges from 10^3 to 3×10^4 km. As required, the average values of q are all close to the Anderson & Athay (1989a) value of 4.5×10^9 ergs-g^{-1}-sec^{-1}. q is independent of height in agreement with the model prediction of Anderson & Athay (1989a). The pressure, shown in Fig. 13, reaches its maximum value near the middle of the elements where the heating rates are largest.

5.2.4. Resistivity and plasma β

The values of the Pedersen resistivity for solutions a - d are $1.6 \times 10^{-6}, 3.1 \times 10^{-5}, 9.3 \times 10^{-5}$, and 3.5×10^{-4} sec. The resistivity increases with the size of the magnetic element. The larger elements have larger resistivities due to their lower proton and hydrogen densities. The ranges of β for solutions a - d are $\sim$ 4 - 23%, 10 - 27%, 7 - 18%, and 5 - 16%.

6. Summary and discussion

It is proposed that large scale electric currents exist in the middle chromosphere and make a major contribution to its heating through resistive dissipation. The currents flow orthogonal to the magnetic field in the weakly ionized, strongly magnetized middle chromospheric gas. The current is carried mainly by protons, with a significant contribution possibly coming from heavier positive ions as discussed by Goodman (1995). The driver of the current is proposed to be a convection electric field generated by flow of the mostly neutral hydrogen gas perpendicular to the magnetic field. The total flow velocity is almost parallel to $\boldsymbol{B}$. Its relatively small component perpendicular to $\boldsymbol{B}$ generates the convection electric field which drives the current. The vertical component of the velocity field predicted by the model is downward towards the photosphere. The strength of the driving convection electric field is $V_\perp B/c$, so the volume heating rate is $(V_\perp B/c)^2/\eta$ which indicates that, for a given resistivity, sufficiently large values of both $V_\perp$ and B are necessary in order that there be significant heating.

The origin of the velocity field is not addressed by the model. The velocity field may be causally related to several dynamic processes such as return flow from spicules, the relative motion between rising magnetic loops and the surrounding plasma, flows generated by MHD wave propagation, downflows resulting from radiative condensation in the upper atmosphere, and flows generated by magnetic induction effects caused by the motion of the footpoints of chromospheric magnetic loops anchored in the underlying photosphere. Any process which drives flow orthogonal to the magnetic field must lead to some heating by the proposed heating mechanism.

The magnetic elements in which the heating takes place have a closed loop geometry and are embedded in a stronger, larger scale potential magnetic field. The field of the element is a few gauss while the potential field strength is 10 - 20 times larger. Since all of the heating takes place in the elements only the loop like geometry of the elements may be visible in observations of net radiative loss. However, since the potential field is much stronger than the field of the element, only the potential field is visible in magnetometer observations with insufficient resolution, leading to the appearance that the middle chromospheric magnetic field is current free, and hence force free. The heating

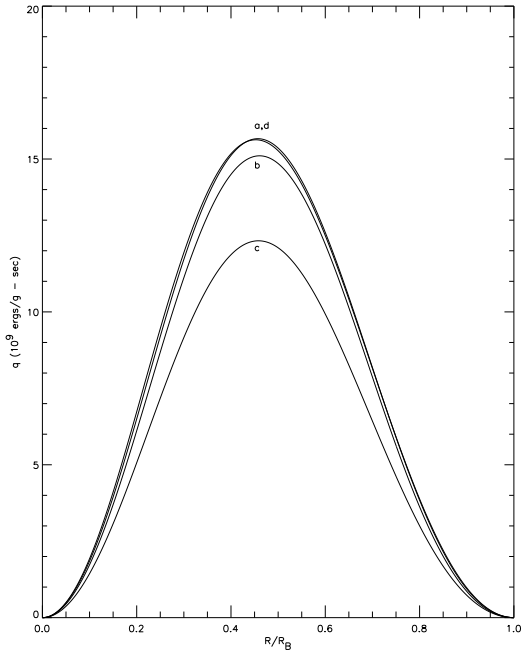

Fig. 11. Heating rate per unit mass vs. $R/R_{\rm B}$. q is independent of height. The average values of q for solutions a - d are $(7.2, 6.9, 5.6, 7.2) \times 10^9$ ergs-g^{-1}-sec^{-1}.

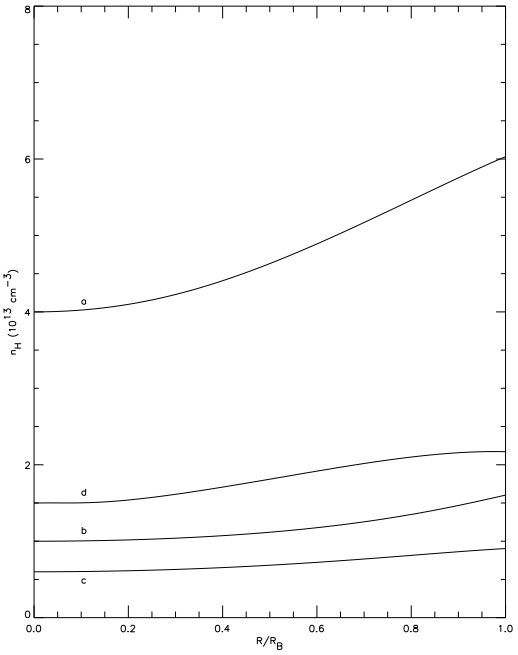

Fig. 12. Hydrogen density vs. $R/R_{\rm B}$ for $(z - z_0) = 0$. (d) $n_{\rm H} \times 10$. All other profiles are unscaled. The scale height of $n_{\rm H}$ is the same as for the pressure in Fig. 13. The average values of $n_{\rm H}$ for solutions a - d are $(5.1, 1.3, 0.8, 0.2) \times 10^{13}$ cm^{-3}.

rates per unit mass and volume are peaked near the midpoint of the magnetic elements where the field of the elements is almost horizontal. Hence sufficiently high spatial resolution intensity observations of the emitting regions are predicted to reveal a loop like geometry with an intensity maximum near the middle of the loop. These considerations apply only to isolated elements and their associated potential field. The field in the actual chromosphere is in general expected to be a superposition of several magnetic element and potential field distributions, making the identification and study of their individual properties more difficult. Isolated magnetic loops are, however, observed.

The magnetic elements with $R_{\rm B}$ = 1000 and 5000 km are intended to represent magnetic elements which are confined to, and heat, the middle network chromosphere. The magnetic elements with $R_{\rm B} = 10^4$ and 3×10^4 km are intended to represent magnetic elements in the middle internetwork chromosphere that comprise the magnetic canopy. These elements are imagined to be based in the network and to extend over the interior of supergranules. The network elements have higher densities than the internetwork elements. The network elements have a heating rate per unit volume nearly one order of magnitude larger than that of the internetwork elements, and so are expected to radiate much more intensely per unit volume than the internetwork elements. However, due to the relatively low density of the internetwork elements, the horizontal profile, and hence the average value, of the heating rate per unit mass is nearly the same for the network and internetwork elements.

Since the model is steady state it cannot make direct contact with the effects of wave generation, propagation, and dissipation that may be important for chromospheric heating. The heating mechanism proposed here may be relevant to middle chromospheric heating on time scales longer than the 3 and 5 - 20 minute periods of chromospheric intensity oscillations commonly observed in the chromospheric internetwork and network, respectively (von Uexküll & Kneer 1995; Bocchialini et al. 1994; Lites 1994; Lites et al. 1993; Kneer & von Uexküll 1993; Kulaczewski 1992; Deubner & Fleck 1990). It may also be the case that the solutions presented here are representative of the state of the plasma during the main driving phase of heating by wave dissipation. An important unanswered question is: to what extent is the total net radiative loss of the chromosphere modulated by the observed oscillations? If the modulation is large then the driver of the heating mechanism oscillates with the observed periods. If the modulation is small then the primary driver of the heating varies on time scales longer than the observed periods, and the observed oscillations are a small perturbation on a relatively steady state heating mechanism. It may also be that there are several drivers acting over a wide range of time scales, and that all of them contribute substantially to middle chromospheric heating.

There is a clear connection between intensity oscillations (bright points) in the lower chromospheric network and the network magnetic field (Suematsu et al. 1995; Cook et al. 1983), although there appears to be a class of network bright points associated with spicules at $T \sim 10^4$ K which are not correlated with changes in the network magnetic field (Suematsu et al. 1995). These observations suggest that the model be extended to apply to the lower chromosphere, and to include time depen-

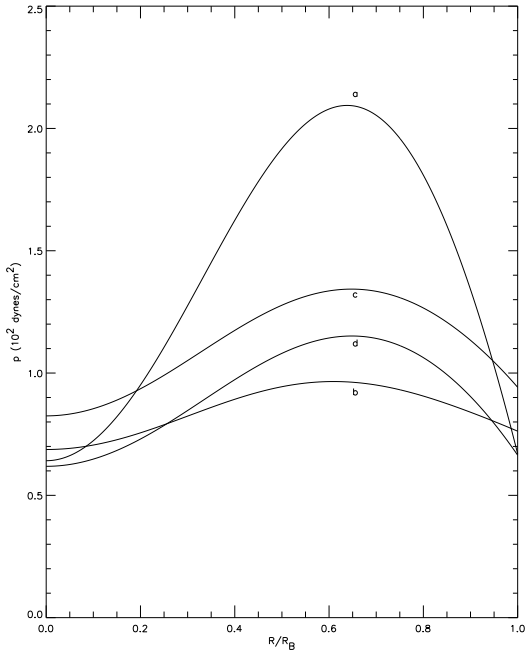

Fig. 13. Pressure vs. $R/R_{\rm B}$ for $(z - z_0)$ = 0. The scale height of p for solutions a - d is 350, 1500, 3000, and 9000 km. The average values of p for solutions a - d are 159.7, 88.2, 119.0, and 97.9 dynes-cm^{-2}.

dence to estimate the degree to which oscillations modulate the heating rate due to the dissipation of electric currents that flow orthogonal to the magnetic field in the weakly ionized lower chromosphere.

At the base of the upper chromospheric network quasi - steady downflows of $\sim$ 10 km-sec^{-1} are observed together with periodic waves and what appears to be turbulent motion (Kneer & von Uexküll 1986). In the chromospheric internetwork waves may propagate from the photosphere up to the temperature minimum where they are damped, heating the plasma and generating waves in the magnetic canopy in the middle chromosphere which may propagate along field lines down into the lower chromospheric network contributing to its heating (Bocchialini & Baudin 1995; Deubner & Fleck 1990; Fleck & Deubner 1989). This scenario is consistent with observations of Lites et al. (1993) which indicate that oscillations in the low internetwork chromosphere are strongly correlated with oscillations in the underlying photosphere, but that oscillations in the low network chromosphere are not correlated with oscillations in the underlying photosphere. It may be that excitation of waves in the canopy is related to the flows and associated convection electric fields and currents considered here.

It is proposed that the model presented here isolates the essential features of a heating mechanism which operates in the weakly ionized middle chromosphere. Although the model is steady state, the heating mechanism it models can operate as a dynamic process. A temperature minimum region and the associated chromospheric temperature rise appear to exist over at least 90% of the solar surface (Athay & Dere 1990). Magnetic bipoles emerge continuously from the photosphere into the chromosphere over the entire solar surface, and are immersed in the convection of the weakly ionized lower atmosphere. Localized heating by a mechanism similar to the one considered here, in a distribution of these bipoles over the surface of the Sun, may at least partially account for the globally observed chromospheric temperature rise.

Acknowledgements. The author thanks Stuart Jordan in the Laboratory for Astronomy and Astrophysics at NASA Goddard for important discussions of the material presented in this paper. The author thanks Steven Curtis and William Mish in the Laboratory for Extraterrestrial Physics at NASA Goddard for their support of this work.

References

Anderson, L.S. 1989, ApJ, 339, 558
Anderson, L.S. & Athay, R.G. 1989a, ApJ, 336, 1089
Anderson, L.S. & Athay, R.G. 1989b, ApJ, 346, 1010
Athay, R.G. 1981, in The Sun as a Star, ed. S.D. Jordan (NASA SP-450), 85
Athay, R.G. & Dere, D.P. 1990, ApJ, 358, 710
Athay, R.G. & Dere, D.P. 1991, ApJ, 381, 323
Athay, R.G., Gurman J.B. & Henze, W. 1983, ApJ, 269, 706
Athay, R.G., Gurman, J.B., Henze, W. & Shine, R.A. 1983, ApJ, 265, 519
Athay, R.G., Gurman, J.B., Henze, W. & Shine, R.A. 1982, ApJ, 261, 684
Avrett, E.H. 1984, in Chromospheric Diagnostics and Modeling, ed. B.W. Lites (Sunspot, NM: National Solar Observatory)
Balescu, R. 1988, *Transport Processes in Plasmas, Vol. 1* (North Holland, New York)
Bocchialini, K. & Baudin, F. 1995, A&A, 299, 893
Bocchialini, K., Vial, J-C & Koutchmy, S. 1994, ApJ, 423, L67
Book, D.L. 1990, NRL Plasma Formulary (Naval Research Laboratory), 39
Briand, C. & Solanki, S.K. 1995, A&A, 299, 596
Carlsson, M. & Stein, R.F. 1992, ApJ, 397, L59
——————— 1994, in Chromospheric Dynamics, ed. M. Carlsson (Inst. of Theoretical Astrophysics, University of Oslo, Norway), 47
——————— 1995, ApJ, 440, L29
Chang, E.S. & Schoenfeld, W.G. 1991, ApJ, 383, 450
Cook, J.W., Brueckner, G.E. & Bartoe, J.-D.F. 1983, ApJ, 270, L89
Cook, J.W. & Ewing, J.A. 1990, ApJ, 355, 719
Chapman, S. & Cowling, T.J. 1970, The Mathematical Theory of Non-Uniform Gases (Cambridge), 366
Cram, L.E. & Damé, L. 1983, ApJ, 272, 355
Dere, K.P., Bartoe, J.-D.F. & Brueckner, G.E. 1984, ApJ, 281, 870
Dere, K.P., Bartoe, J.-D.F. & Brueckner, G.E. 1983, ApJ, 267, L65
Deubner, F.-L. & Fleck, B. 1990, A&A, 228, 506
Faurobert - Scholl, M. 1992, A&A, 258, 521
Faurobert - Scholl, M. 1993, A&A, 268, 765
Faurobert - Scholl, M. 1994, A&A, 285, 655
Faurobert - Scholl, M., Feautrier, N., Machefert, F., Petrovay, K. & Spielfiedel, A. 1995, A&A, 298, 289
Feldman, U. 1993, ApJ, 411, 896
Fleck, B. & Duebner, F.-L. 1989, A&A, 224, 245
Foing, B., Bonnet, R.-M., Bruner, M. 1986, A&A, 162, 292
Gebbie, K.B., Hill, F., Toomre, J., November, L.J., Simon, G.W., Gurman, J.B., Shine, R.A., Woodgate, B.E., Athay, R.G., Bruner Jr., E.C., Rehse, R.A. & Tandberg-Hanssen, E.A. 1981, ApJ, 251, L115

Goodman, M.L. 1995, ApJ, 443, 450
Goodman, M.L. 1996, ApJ, 463, 784
Grossmann - Doerth, U. & Schmidt, W. 1992, A&A, 264, 236
Hasan, S.S. & Keil, S.L. 1984, ApJ, 283, L75
Kalkofen, W. 1989, ApJ, 346, L37
Kalkofen, W. 1996, ApJ, 468, L69
Karovska, M. & Habbal, S.R. 1991, ApJ, 371, 402
Keller, C.U., Deubner, F.-L., Egger, U., Fleck, B. & Povel, H.P. 1994, A&A, 286, 626
Kneer, F. & von Uexküll, M. 1993, A&A, 274, 584
Kulaczewski, J. 1992, A&A, 261, 602
Lin, H. 1995, ApJ, 446, 421
Lites, B.W., Rutten, R.J. & Kalkofen, W. 1993, ApJ, 414, 345
Lites, B.W. 1994, in Chromospheric Dynamics, ed. M. Carlsson (Inst. of Theoretical Astrophysics, University of Oslo, Norway), 1
Maltby, P., Avrett, E.H., Carlsson, M., Kjeldseth-Moe, O., Kurucz, R.L. & Loeser, R. 1986, ApJ, 306, 284
Metcalf, T.R., Canfield, R.C., Hudson, H.S., Mickey, D.L., Wulser, J.P., Martens, P.C.H. & Tsuneta, S. 1994, ApJ, 428, 860
Muller, R. 1995, Sol. Phy., 100, 237
November, L.J., Toomre, J., Gebbie, K.B. & Simon, G.W. 1979, ApJ, 227, 600
Rammacher, W. & Ulmschneider, P. 1992, A&A, 253, 586
Rutten, R., & Uitenbroek, H. 1991, Sol. Phys., 134, 15
Schussler, M. 1992, in The Sun: A Laboratory for Astrophysics, ed. J.T. Schmelz & J.C. Brown (Kluwer: NATO ASI Series)
Heinzel, P. & Schmieder, B. 1994, A&A, 282, 939
Sivaraman, K.R. & Livingston, W.C. 1982, Sol. Phys., 80, 227
Solanki, S.K. 1993, Space Science Rev., 63, 1
Solanki, S.K., Bruls, J.H.M.J., Steiner, O., Ayres, T., Livingston, W. & Uitenbroek, H. 1994, in Solar Surface Magnetism, R.J. Rutten & C.J. Schrijver (eds.), NATO ASI Series C433, Kluwer, Dordrecht, 91
Solanki, S.K. & Steiner, O. 1990, A&A, 234, 519
Suematsu, Y., Wang, H. & Zirin, H. 1995, ApJ, 450, 411
Title, A.M. & Berger, T.E. 1996, ApJ, 463, 797
Vernazza, J.E., Avrett, E.H. & Loeser, R. 1981, ApJS, 45, 635
von Uexküll, M. & Kneer, F. 1995, A&A, 294, 252
Zwann, C. 1981, in The Sun as a Star, ed. S.D. Jordan (NASA SP-450), 167
——— 1987, in ARA&A (Palo Alto: Annual Reviews), 25, 83

This article was processed by the author using Springer-Verlag LaTeX A&A style file *L-AA* version 3.